Interactions between Arctic sea ice drift and strength modelled by NEMO-LIM3.6

David Docquier[1], François Massonnet[1,2], Antoine Barthélemy[1], Neil F. Tandon[3], Olivier Lecomte[1], and Thierry Fichefet[1]

[1]Université catholique de Louvain (UCL), Earth and Life Institute (ELI), Georges Lemaître Centre for Earth and Climate Research (TECLIM), Louvain-la-Neuve, Belgium
[2]Barcelona Supercomputing Center - Centro Nacional de Supercomputación (BSC-CNS), Earth Sciences Department, Barcelona, Spain
[3]Environment and Climate Change Canada (ECCC), Climate Research Division, Toronto, Canada

Correspondence to: david.docquier@uclouvain.be

Preliminary remark for the revised manuscript (not the track change version):

- corrections related to Referee 1 are in blue

- corrections related to Referee 2 are in red

- other corrections are in orange.

Abstract. Sea ice cover and thickness have substantially decreased in the Arctic Ocean since the beginning of the satellite era. As a result, sea ice strength has been reduced, allowing more deformation and fracturing and leading to increased sea ice drift speed. We use the version 3.6 of the global ocean-sea ice NEMO-LIM model (Nucleus for European Modelling of the Ocean coupled to the Louvain-la-Neuve sea Ice Model), satellite, buoy and submarine observations, as well as reanalysis data over the period from 1979 to 2013 to study these interactions. Overall, the model agrees well with observations in terms of sea ice extent, concentration and thickness. Although the seasonal cycle of sea ice drift speed is reasonably well reproduced by the model, the recent positive trend in drift speed is weaker than buoy observations in summer. NEMO-LIM3.6 is able to capture the relationships between the seasonal cycles of sea ice drift speed, concentration and thickness, with higher drift speed for both lower concentration and lower thickness, in agreement with observations. Sensitivity experiments are carried out by varying the initial ice strength, and these show that higher values of ice strength lead to lower sea ice deformation and lower sea ice thickness. The methodology proposed in this analysis provides a benchmark for a further model intercomparison related to the interactions between sea ice drift speed and strength, which is especially relevant in the context of the upcoming Coupled Model Intercomparison Project 6 (CMIP6).

1 Introduction

The motion or drift of sea ice results from a balance of wind stress, ocean stress, ice internal stress, Coriolis force and ocean surface tilt. Scale analysis shows that the main drivers of drift are the first three terms, and that both Coriolis force and ocean

surface tilt are an order of magnitude smaller (Steele et al., 1997; Leppäranta, 2011). For individual ice floes and for ice fields with low compactness, ice internal stress is generally neglected: sea ice is in free drift. Otherwise, ice internal stress is an important driver of sea ice motion and is a key element of the interactions between sea ice drift speed and strength described hereafter. In this paper, we focus on the Arctic Ocean, for which a sufficient network of observations is available.

5   At large scale, sea ice strength mainly depends on two quantities, namely sea ice concentration (defined as the relative amount of ocean area covered by sea ice) and sea ice thickness. A decrease in concentration or thickness, as observed in recent decades in the Arctic Ocean (Stroeve et al., 2012; Vaughan et al., 2013; Lindsay and Schweiger, 2015), leads to a reduced ice strength and internal stress, which allows more deformation and fracturing within the ice, hence larger sea ice drift speed (Rampal et al., 2011; Spreen et al., 2011; Kwok et al., 2013). This in turn could provide higher export of sea ice out of the

10   Arctic Basin (Rampal et al., 2011), resulting in lower sea ice concentration and further thinning (Langehaug et al., 2013). However, this hypothetical positive feedback, which we call 'drift-strength feedback' throughout this paper, has been poorly studied and its existence has not been shown in observations.

A clear increase in Arctic sea ice drift speed has been detected since the 1950s using buoy observations and satellite measurements (Häkkinen et al., 2008; Rampal et al., 2009, 2011; Spreen et al., 2011; Vihma et al., 2012; Kwok et al., 2013; Olason

15   and Notz, 2014). While increased wind speed seems to be the likely cause of the increase in sea ice motion before 1990, the reduced ice strength (caused by reduced thickness and concentration) is the dominant driver since then (Döscher et al., 2014). It has been suggested that an increase in drift speed leads to higher sea ice export from the Arctic Basin, which mainly occurs through Fram Strait. However, a distinction needs to be made between area and volume exports: area export is the product of sea ice drift speed, concentration and transect length, while volume export is the product of area export and ice thickness.

20   Several studies show an increase of ice area export at Fram Strait since the late 1970s (Langehaug et al., 2013; Krumpen et al., 2016; Smedsrud et al., 2016), while Kwok et al. (2013) show a small decrease between 1982 and 2009. In terms of volume export, the amount of studies is limited by the relatively low ice thickness temporal coverage at Fram Strait. Spreen et al. (2009) show no significant change in ice volume export between 1990 and 2008. The review from Döscher et al. (2014) addresses this question and concludes that there is no significant long-term trend in sea ice area export due to a balance between increased

25   drift speed and decreased concentration, while volume export slightly falls due to a decreased sea ice thickness. A summary of these studies related to drift speed trend and its cause as well as sea ice export at Fram Strait is provided in Table 1.

Olason and Notz (2014) investigate the interactions between Arctic sea ice drift speed, concentration and thickness using satellite and buoy observations. They show that both seasonal and recent long-term changes in sea ice drift are primarily correlated to changes in sea ice concentration and thickness. On seasonal time scales, when sea ice concentration is low (from

30   June to November), drift speed increases with decreasing concentration, while for high concentration (from December to March), drift speed changes are largely driven by changes in thickness (higher drift speed with lower thickness).

An analysis of sea ice output from the Coupled Model Intercomparison Project 3 (CMIP3) multi-model dataset suggests that thicker and more packed sea ice drifts faster, contrary to what is observed (Rampal et al., 2011). The same study also shows that models with a stronger long-term thinning trend do not exhibit faster drift speed, suggesting that the coupling between

drift and strength is underestimated in CMIP3 models. According to the authors, this could explain the too low trends in sea ice area, thickness and drift speed.

The main goal of this study is to investigate the interactions between Arctic sea ice drift speed and strength using version 3.6 of the Nucleus for European Modelling of the Ocean coupled to the Louvain-la-Neuve sea Ice Model (NEMO-LIM3.6). We first apply the methodology developed by Olason and Notz (2014) to the model to see how changes in ice drift speed are related to changes in ice concentration and thickness throughout the year. However, good agreement between the modelled and observed drift-strength relationships is not a guarantee that the model is able to capture drift-strength interactions. Thus, we carry on additional sensitivity experiments where initial ice strength is varied, and we investigate the impact on the resulting drift speed, concentration and thickness of sea ice. The methodology proposed in this analysis provides a benchmark for further model intercomparison related to drift-strength interactions and could be used in the analysis of sea ice outputs from the upcoming High Resolution Model Intercomparison Project (HighResMIP) (Haarsma et al., 2016) and CMIP6 Sea-Ice Model Intercomparison Project (SIMIP) (Notz et al., 2016).

In Section 2 we describe the model, the observations as well as the diagnostics and metrics. Then, results from the model evaluation against different observational and reanalysis datasets are presented (Section 3.1). Section 3.2 details the interactions between drift speed and strength on seasonal time scales. Results from the sensitivity experiments are shown in Section 3.3. These results are discussed in Section 4. Finally, a summary is provided in Section 5.

2   Methodology

2.1   Model description and sensitivity experiments

The model used in this study is version 3.6 of the global ocean-sea ice coupled model NEMO-LIM (SVN revision 6631). The ocean component NEMO3.6 is a finite difference, hydrostatic, primitive equation model (Madec, 2016). The sea ice component LIM3.6 is a dynamic-thermodynamic model that uses the elastic-viscous-plastic (EVP) rheology on a C-grid and includes an explicit ice thickness distribution (ITD) (Vancoppenolle et al., 2009; Rousset et al., 2015).

The atmospheric forcing is the Drakkar Forcing Set (DFS) 5.2 (Dussin et al., 2016), which is based on the ERA-Interim atmospheric reanalysis dataset. The model is run on the global tripolar eORCA1 grid (about $1°$ spatial resolution) from January 1958 to December 2015. Model outputs that are used in this study are sea ice concentration, thickness and velocity components over the period 1979-2013. This period is chosen to match the satellite period. Sea ice thickness used in this study is the sea ice volume per grid cell area taking into account open water (named 'sivol' according to SIMIP nomenclature) rather than the actual thickness ('sithick'), since the former is more physical in representing global interactions between sea ice dynamics and thermodynamics, and this is the variable used in the formulation of sea ice strength detailed below.

Four different simulations are performed in order to test the sensitivity of sea ice drift speed, thickness and concentration to changes in initial sea ice strength P. The latter is computed as a function of ice thickness h and concentration A using the

formulation of Hibler (1979):

$$P = P^* h \exp[-C(1-A)],$$ (1)

where C (= 20) and P^* are fixed empirical constants. Five different values of P^* (5.5, 20, 27.5, 45 and 100 kN m^{-2}) are used in order to perform sensitivity experiments to test how a change in the strength parameterisation impacts the ice drift speed,

5 concentration and thickness. The experiment with $P^* = 20$ kN m^{-2} is the control simulation that is analysed in Sections 3.1 and 3.2. The results from the other four experiments are presented in Section 3.3.

The value of $P^* = 20$ kN m^{-2} is the commonly used value in NEMO-LIM3.6 and has been chosen through tuning of mean sea ice thickness and mean Fram Strait ice export (Vancoppenolle, personal communication). This is also the value used in the viscous-plastic models of SIMIP (Kreyscher et al., 1997) as well as in more recent modelling studies (Lipscomb et al.,

10 2007; Juricke et al., 2013). Hibler and Walsh (1982) find that $P^* = 27.5$ kN m^{-2} provides the best agreement between their 222 km-resolution sea ice model and observations from the Soviet ice station NP-22 in terms of mean drift rates in 1974-1975. Tremblay and Hakakian (2006) find that the most likely value of P^* lies in the range 30-45 kN m^{-2} based on satellite observations. Therefore, the value of P^* in Eq. (1) is highly uncertain and not a single value is considered as a reference (Feltham, 2008). The different sensitivity experiments carried out in this study account for this uncertainty.

15 The experiment with $P^* = 5.5$ kN m^{-2} provides lower ice strength P than the control simulation ($P^* = 20$ kN m^{-2}) for a given thickness. It is the lowest value used by Steele et al. (1997) in their model sensitivity study, corresponding to the value of 27.5 kN m^{-2} (Hibler and Walsh, 1982) divided by 5. The experiment with $P^* = 27.5$ kN m^{-2} gives higher ice strength P than the control simulation and corresponds to the value found by Hibler and Walsh (1982). The experiment with $P^* = 45$ kN m^{-2} is the largest value of the likely range found by Tremblay and Hakakian (2006). The experiment with $P^* = 100$ kN m^{-2} is

20 close to the highest value of Steele et al. (1997). Figure 1 shows how sea ice strength varies as a function of sea ice thickness and concentration for the five P^* values.

2.2 Reference products

In this study, we use several observational and reanalysis datasets for a given variable in order to evaluate model results, following the recommendations of Notz (2015) and Massonnet et al. (2016).

25 ### 2.2.1 Sea ice drift speed

For sea ice drift speed, the International Arctic Buoy Programme (IABP) C buoy dataset is retrieved from the National Snow and Ice Data Center (NSIDC) (Tschudi et al., 2016). This dataset provides 12-hourly sea ice velocity vectors derived from buoy positions over the period extending from 1979 to 2015. Ice motion derived from buoys is more accurate than that obtained from satellites (error of less than 1 cm s^{-1} for the average velocity over 24 h according to NSIDC), but the coverage is very limited

30 and the number of buoys and their locations varies from year to year. In addition, buoys have not been placed on ice in the Eastern Arctic. The daily mean sea ice drift speed is computed for each buoy from 12-hourly data.

We also include the merged product from Tschudi et al. (2016), which provides daily sea ice motion vectors on the Equal-Area Scalable Earth (EASE) Grid with a resolution of 25 km from 1979 to 2015. This dataset, available on the NSIDC website, is a compilation of velocity vectors from IABP buoy data, satellite observations from Advanced Microwave Scanning Radiometer - Earth Observing System (AMSR-E), Advanced Very High Resolution Radiometer (AVHRR), Scanning Multi-channel Microwave Radiometer (SMMR), Special Sensor Microwave/Imager (SSM/I) and Special Sensor Microwave Imager Sounder (SSMIS), as well as NCEP-NCAR reanalysis. The different sources of data are combined through a weighting that depends on the accuracy of each dataset. This merged product suffers from artifacts of the method used to incorporate buoy data, especially in terms of ice divergence and convergence (Szanyi et al., 2016). In our manuscript, we call this product 'NSIDC'.

We use the low resolution sea ice drift product (OSI-405-b) from the European Organisation for the Exploitation of Meteorological Satellites Ocean and Sea Ice Satellite Application Facility (EUMETSAT OSI SAF, 2015b; Lavergne et al., 2010). This dataset covers the period from October 2006 to present. No data is available from May to September (inclusive) for the Arctic region due to high atmospheric liquid water content and to ice surface melting. Despite this low temporal coverage compared to other sea ice drift products, the quality of OSI SAF data is superior to other satellite products based on a recent uncertainty estimate (Sumata et al., 2014). This dataset combines satellite measurements of both the brightness temperature using passive microwave instruments from SSM/I, SSMIS, AMSR-E and Advanced Microwave Scanning Radiometer 2 (AMSR2) and the radar backscatter using Advanced Scatterometer (ASCAT). Sea ice drift vectors are provided every 2 days at a spatial resolution of 62.5 km, and we calculate daily mean drift speed from these data. We compared modelled drift speed averaged over two days to original OSI SAF data but we did not find any significant difference. Since we mainly compare the modelled sea ice drift speed to buoy data instead of satellite data (which have a lower temporal coverage), we have decided to keep daily averages of sea ice drift speed as a benchmark for comparison.

2.2.2 Sea ice concentration

For sea ice concentration, the global reprocessed dataset (OSI-409-a) from OSI SAF (EUMETSAT OSI SAF, 2015a) is used. It covers the period from October 1978 to April 2015 using passive microwave data from SMMR, SSM/I and SSMIS. The OSI SAF algorithm to retrieve concentration from brightness temperature is a linear combination of the Bootstrap algorithm in frequency mode over open water (Comiso, 1986; Comiso et al., 1997) and the Bristol algorithm over ice (Smith, 1996). This is one of the best concentration algorithms in terms of precision (standard deviation) according to a recent evaluation (Ivanova et al., 2015). The spatial resolution for this dataset is 10 km. We compute the monthly mean concentration from daily data.

We also retrieve the monthly mean sea ice concentration (1979-2015) computed from the AMSR-E Bootstrap algorithm with daily varying tie-points (Comiso, 2015). This dataset is derived using measurements from SMMR, SSM/I and SSMIS. Due to orbit inclination, data do not cover the region north of 84.5 °N for SMMR and 87.2 °N for SSM/I and SSMIS. Data are gridded on the SSM/I polar stereographic grid with a 25 km resolution. Largest errors related to this dataset are found in summer when melt is underway.

2.2.3 Sea ice thickness

For sea ice thickness, we use the multiple regression model of Rothrock et al. (2008), based on 34 US Navy submarine cruises spanning the period 1975-2000 within the Scientific Ice Expeditions (SCICEX) box. This dataset includes more than 2000 records of sea ice draft (mostly in spring and autumn) measured from the first-return echo. A positive mean bias of 0.29 m in ice draft is identified by Rothrock and Wensnahan (2007) and is taken into account in our study. Sea ice thickness is derived from the draft using the methodology of Rothrock et al. (2008).

The gridded data at a spatial resolution of 25 km from ten Ice, Cloud, and land Elevation Satellite (ICESat) campaigns is also used (Kwok et al., 2009). The Geoscience Laser Altimeter System (GLAS) is the laser altimeter on board ICESat that measures sea ice freeboard height, from which sea ice thickness is derived using snow depth and densities of ice, snow and water. The coverage period is limited to the months of October-November and February-March starting in late September 2003 and ending in March 2008. The Kwok et al. (2009) dataset provides the mean sea ice thickness for each of the ten campaigns. The mean absolute uncertainty of sea ice thickness derived from ICESat is 0.21 m in October-November and 0.28 m in February-March (Zygmuntowska et al., 2014).

Due to the spatial and temporal gaps of sea ice thickness measurements and the high uncertainty inherent to thickness retrievals (Stroeve et al., 2014; Zygmuntowska et al., 2014), we also use monthly mean thickness derived from the Pan-Arctic Ice-Ocean Modeling and Assimilation System (PIOMAS) over the period 1979-2013. PIOMAS is a multi-category thickness and enthalpy distribution sea ice model coupled to the Parallel Ocean Program developed at the Los Alamos National Laboratory (Zhang and Rothrock, 2003). The model assimilates observed sea ice concentration and sea surface temperature and is driven by daily NCEP-NCAR reanalysis surface forcing fields. The mean horizontal resolution in the Arctic is 22 km. PIOMAS data are primarily model-generated, and must therefore be interpreted with caution. Nevertheless, sea ice thickness from PIOMAS agrees well with ICESat data over the region for which submarine data are available (Schweiger et al., 2011) and constitutes a valuable tool in our analysis. Given the uncertainties of both observational products and PIOMAS, using all of the products together allows us to obtain a range of 'reference values' that is more reliable than the range based on observational products alone.

2.3 Diagnostics and metrics

A diagnostic is a measure of one characteristic of a model or an observational dataset, while a metric is a scalar number that compares a diagnostic to some reference (typically observations). In this study, we use both 'standard' diagnostics as well as process-based diagnostics and metrics. The standard diagnostics that we use are:

– sea ice extent, defined as the total area of ocean with sea ice concentration higher than 0.15

– sea ice area, which is the total area of sea ice cover, computed due to uncertainties linked to sea ice extent (Notz, 2014)

– sea ice concentration, which is the relative amount of ocean area covered by sea ice

– sea ice thickness, defined as the sea ice volume per grid cell area

– sea ice drift speed, which is the velocity of sea ice computed at the daily time scale.

It is important to note that for drift speed, all values given in this study are computed from the daily mean components of sea ice velocity u_d and v_d:

$$D_d = \sqrt{u_d^2 + v_d^2}. \tag{2}$$

where D_d is the daily mean drift speed. Monthly mean drift speed computed from the daily components of sea ice velocity

5 is approximately twice higher than monthly mean drift speed computed from monthly components of sea ice velocity with NEMO-LIM3.6 due to higher temporal variability at the daily timescale (Fig. 2). A recent analysis also shows that such a factor of two is also apparent within the CMIP5 models (Tandon et al., submitted). Using daily components is more accurate for our study because we can capture synoptic-scale variability.

From daily values of these standard diagnostics, we compute monthly means temporally averaged over the period 1979-

10 2013 and monthly trends (i.e. linear regression slopes) over the same period. The maps shown in this paper (Figs. 4, 5, 7, 10) provide monthly means averaged over three consecutive months for winter (January, February, March) and summer (July, August, September) for each grid cell. The plots of mean seasonal cycles (Figs. 3, 6, 9, 11) provide spatial means over the SCICEX box (Rothrock et al., 2008), which is also the domain used by Olason and Notz (2014) in their study. The SCICEX box is representative of sea ice processes happening in the Central Arctic region and is well covered by observational datasets

15 of sea ice concentration, thickness and drift speed. All maps in this study show the contours of the SCICEX box. We have also tested computing spatial means over a much wider domain taking into account all grid cells between 50 and 90 °N with a concentration threshold of $A \geq 0.15$. Unless specifically mentioned in the text, the default domain that is used in the following sections is the SCICEX box. Since IABP buoy data are not gridded, we use all buoys within the SCICEX box to compute the spatial mean over that region. We acknowledge that comparing buoy and model drift speed has to be done with caution, as

20 buoys measure the drift speed at one particular location while the model is meant to give the grid-cell average. For computing spatial means, a weight is given to each grid cell proportional to the grid cell area.

Based on the 'standard' diagnostics described above, we use two process-based diagnostics in order to quantify the ability of NEMO-LIM3.6 to capture the interactions between sea ice drift speed and strength in the Arctic. The first process-based diagnostic is a scatter plot of sea ice drift speed against sea ice concentration for each month of the mean seasonal cycle as in

25 Olason and Notz (2014). The second diagnostic is similar to the first diagnostic with sea ice thickness instead of concentration. All values are spatially averaged over the SCICEX box and temporally averaged over the period 1979-2013. A key difference with Olason and Notz (2014) is that we do not normalise drift speed by wind friction speed since our findings were not sensitive to such normalisation. These two diagnostics are presented in Figs. 8 and 13.

Based on the previous process-based diagnostics, four metrics are computed over the mean seasonal cycle. The first metric

30 s_A measures the ratio of the modelled drift-concentration slope to the observed drift-concentration slope. The closer the ratio to 1, the closer the model to the observations. The second metric s_h is similar to the first metric, except that the ratio involves drift-thickness slopes.

The third and fourth metrics quantify the normalised distances (in %) between the model and observations for both the drift-concentration (ϵ_A) and drift-thickness (ϵ_h) relationships respectively:

$$\epsilon_A = \frac{1}{n}\sum_{i=1}^{n}\sqrt{\left|\frac{A_{m,i}-A_{o,i}}{\overline{A_o}}\right|^2 + \left|\frac{D_{m,i}-D_{o,i}}{\overline{D_o}}\right|^2} \times 100, \tag{3}$$

$$\epsilon_h = \frac{1}{n}\sum_{i=1}^{n}\sqrt{\left|\frac{h_{m,i}-h_{o,i}}{\overline{h_o}}\right|^2 + \left|\frac{D_{m,i}-D_{o,i}}{\overline{D_o}}\right|^2} \times 100, \tag{4}$$

where n is the number of months (i.e. 12), the m and o subscripts stand for 'model' and 'observations' respectively, $\overline{A}$, $\overline{h}$ and $\overline{D}$ are the mean concentration, thickness and drift speed (respectively) over the 12 months.

3 Results

3.1 Model evaluation

The modelled mean seasonal cycle of Arctic sea ice extent is in good agreement with OSI SAF observational reference over the period 1979-2013. However, a too low extent is simulated in August (bias of 1.6 million km^2) (Fig. 3a, solid lines). This feature is similar to Rousset et al. (2015) who use NEMO-LIM3.6 at 2° resolution forced by the CORE normal year forcing proposed by Large and Yeager (2009), which is based on a combination of NCEP/NCAR reanalyses and diverse satellite products and superimposes the 1995 synoptic variability on the mean 1984–2000 seasonal cycle (we use a resolution of 1° and DFS5.2 forcing). The amplitude of the modelled seasonal cycle of sea ice area is higher than the observed one (Fig. 3a, dashed lines). Note that satellite observations perform better in winter compared to summer due to the presence of melt ponds in summer (Ivanova et al., 2015).

The modelled mean seasonal cycle of sea ice concentration is very close to OSI SAF observations for all months, except in August when the model underestimates the mean concentration by ∼0.15 (Fig. 3b). This partly explains the too low extent at that time of the year (Fig. 3a). The Bootstrap algorithm provides higher concentration than OSI SAF, especially in summer, but the spatial coverage is limited due to the absence of data close to the North Pole (Section 2.2 and Fig. 4f). A more careful spatial analysis reveals that the model overestimates sea ice concentration in winter, especially at the ice front (Figs. 4a, 4b, 4c). Furthermore, the model clearly underestimates the observed concentration in the Central Arctic in summer (Figs. 4d, 4e, 4f).

The mean seasonal cycle of sea ice thickness modelled by NEMO-LIM3.6 underestimates the seasonal cycle derived from submarine observations and is in better agreement with PIOMAS with a maximum in May and a minimum in September (Fig. 3c). Compared to PIOMAS, the model overestimates ice thickness when ice is thicker (January to July) and slightly underestimates it when ice is thinner (August to October). We do not show the seasonal cycle of ice thickness from ICESat due to the sparse temporal coverage of these satellite data. However, the model reproduces well the spatial distribution of ICESat thickness with thicker ice north of Greenland and in the Canadian archipelago. The model slightly overestimates the

sea ice thickness provided by ICESat in February, March and April (mean bias of 0.07 m), and underestimates it in October and November (mean bias of -0.65 m).

Compared to IABP buoy observations, the model overestimates sea ice drift speed for all months with higher differences from December to March and for June and July (Fig. 3d). The too strong intensity of the modelled sea ice velocity was already shown with NEMO3.1-LIM2 (Dupont et al., 2015). However, the model captures the seasonality of drift speed with higher values in summer, when concentration and thickness are the lowest, and lower values in winter, when concentration and thickness are high. The minimum modelled drift speed lags the observed minimum by one month (March) and the maximum occurs two months earlier than the observed maximum (September). The NSIDC drift speed from Tschudi et al. (2016) does not show a clear seasonal cycle and has values up to 4 km d^{-1} lower than the IABP product. This is also shown by Olason and Notz (2014) with the previous NSIDC product. Sea ice drift speed from OSI SAF is not shown in Fig. 3d due to the absence of data in summer, but a spatial analysis shows that NEMO-LIM3.6 overestimates these satellite observations during the rest of the year (mean bias of 0.91 km d^{-1}; Fig. 5c). The main patterns of sea ice circulation, i.e. Beaufort Gyre and Transpolar Drift, are reasonably well represented by the model (Figs. 5a and 5d).

Monthly mean trends in sea ice extent are clearly negative all year long in the model and OSI SAF observations, especially in summer, but the model underestimates these trends (Fig. 6a). For sea ice concentration trends, the agreement between the model and observations is relatively good but the model overestimates the negative trend in August and September (Fig. 6b). Monthly mean thickness trends lie within the PIOMAS range but the seasonal cycle amplitude is lower (Fig. 6c). Finally, monthly mean trends in drift speed simulated by the model agree well with IABP from November to June but can not reproduce the positive observed trend from August to October (Fig. 6d). The model produces drift speed trends that are closer to the NSIDC dataset in summer.

Figure 7 shows spatial variations of modelled monthly mean trends in sea ice drift speed and concentration. Interestingly, the summer trend in drift speed is positive in the western part of the SCICEX box and negative in the eastern part (Fig. 7b). This effect is particularly enhanced in August (Fig. 7c), which explains the slightly negative trend in drift speed (-0.18 km d^{-1} decade^{-1}) when averaged over the whole SCICEX box (Fig. 6d). The cause of the negative drift speed trend in August in the eastern Central Arctic is due to the removal of sea ice in this region after 1979, as shown by the modelled trend in sea ice concentration in August (Fig. 7f). When considering grid cells with ice concentration higher than 0.15, the August mean drift trend averaged over the SCICEX box is slightly positive (0.09 km d^{-1} decade^{-1}). Therefore, the model bias in summer drift speed trend is partly due to the absence of summer sea ice in the eastern Central Arctic.

3.2 How does sea ice drift relate to ice strength?

The interactions between sea ice drift speed and strength can be quantified via the relationships between drift speed and concentration on the one hand and drift speed and thickness on the other hand. In this study, we analyse these relationships in terms of mean seasonal cycles. The linear relationship between drift speed and concentration is clear for both the model and the observations when concentration is relatively low (i.e. in summer): the lower the concentration, the higher the drift speed, with slopes significantly different from zero at the 5% level (Fig. 8a). The modelled drift-concentration slope is weaker than

the observed ones (using IABP for drift speed) mainly due to too low mean modelled sea ice concentration in August and too high mean modelled drift speed in March and April. The modelled drift-concentration relationship is in better agreement with the observed IABP/OSI SAF pair (slope ratio $s_A = 0.5$ and normalised distance $\epsilon_A = 3.7\%$) compared to IABP/Bootstrap (s_A = 0.3 and $\epsilon_A = 4.2\%$).

5   The relationship between drift speed and thickness shows a similar general pattern as the drift-concentration relationship with higher drift speed for lower thickness, with significant slopes at the 5% level (Fig. 8b). However, the drift-thickness relationship is more complex with a hysteresis loop for NEMO-LIM3.6, the IABP/Submarines pair and the IABP/PIOMAS pair. From May to September, during the melting season, sea ice thickness decreases and drift speed increases. Then, from September to March, drift speed decreases and thickness increases. The behaviour is slightly different between the model and

10   observations, with a clearer linear relationship from May to September for observations, but the general shape of the scatter plot is similar. For both the model and observations, for a given thickness, the drift speed can take two values depending on the season: a high value in summer when sea ice melts and a low value in winter when sea ice forms and grows.

We also show scatter plots for the monthly mean trends, and these show large differences between the model and the observed pairs (Figs. 8c and 8d). The positive slope of the modelled relationships is largely driven by low trends in summer, while the

15   observations (using IABP for drift speed) show a decrease in drift speed trend with more positive trends in concentration and thickness. The pair using the NSIDC dataset produces a closer drift-thickness slope ratio and normalised distance compared to NEMO-LIM3.6. However, the low trends in modelled drift speed in summer are due more to a progressive removal of sea ice rather than an actual decrease in sea ice motion in past years as previously shown (Section 3.1 and Fig. 7).

The analysis of drift-concentration and drift-thickness relationships demonstrates that NEMO-LIM3.6 captures reasonably

20   well drift-strength interactions on seasonal timescales. Note that relating drift speed to concentration and thickness for every month of the time series (and not only for the mean seasonal cycle) also gives similar slopes with slightly lower model performance ($s_A = 0.5$ and $\epsilon_A = 6.6\%$ compared to the IABP/OSI SAF pair; $s_h = 0.5$ and $\epsilon_h = 7.8\%$ compared to the IABP/PIOMAS pair). The trend relationships are less convincing but two months (August and September) particularly dominate the signal due to a progressive removal of sea ice in the past years within the domain of study.

25 **3.3   Sensitivity to changes in ice strength**

The previous scatter plots (Fig. 8) are valuable to provide insight regarding the interactions between sea ice dynamics and strength (concentration and thickness), but they do not quantify the impact of a change in sea ice strength on the resulting ice thickness and drift speed. In order to do this, we perform experiments in which we vary P* in Eq. (1), as described in Section 2.1 and in Fig. 1.

30   Varying P^* leads to tiny differences in mean sea ice concentration (not shown) but has a significant impact on sea ice thickness and drift speed (Fig. 9). For higher values of P^*, i.e. larger ice strength, the mean sea ice thickness is lower throughout the whole year (Fig. 9a) and the mean drift speed is lower in winter and spring and higher during summer and fall (Fig. 9b).

Increasing ice strength via the P^* parameter leads to lower thickness values (Fig. 9a). A more careful spatial analysis allows us to see that the lower ice thickness with higher P^* appears everywhere in the Arctic and during all months of the year, with

the most visible differences occurring north of Greenland and the Canadian Archipelago where ice is the thickest (Fig. 10). In the experiments with larger (lower) P^*, the mean ice thickness is lower (higher) due to lower (higher) deformation rates (Fig. 11a) and less (more) ice piling up (Fig. 10); this finding is similar as Steele et al. (1997). Deformation rates are computed from strain rate divergence and shear following Eq. (5) from Spreen et al. (2017). However, deformation rates from the experiment with $P^* = 100$ kN m^{-2} are relatively high compared to other experiments, especially in winter (Fig. 11a), despite the relatively low thickness arising from this experiment (Fig. 9a). The net ice production resulting from this experiment, which combines all sea ice mass balance processes described in Rousset et al. (2015), is 1.5 times lower than the four other experiments on average, which all provide a very similar seasonal cycle (Fig. 11b). Therefore, relatively high deformation rates with $P^* = 100$ kN m^{-2} are compensated by relatively low net ice production, which provides low ice thickness. Table 2 provides a summary of mean ice thickness, drift speed, deformation rates and net ice production averaged over the whole period and over the SCICEX box.

The experiments with higher P^* also provide a more uniform sea ice thickness distribution resulting from a higher ice strength. Figure 12 shows the distribution of ice-covered grid cells in each thickness bin for both winter and summer months: the higher the ice strength (higher P^*), the higher the number of grid cells in the modal class (2.5-3 m in winter and 1.5-2.5 m in summer), and the more uniform (i.e. peaked) the thickness distribution.

Higher sea ice drift speed with higher ice strength from June to August, except for $P^* = 100$ kN m^{-2} (Fig. 9b), probably stems from the fact that for higher strength, ice thickness is lower at the beginning of the summer (Fig. 9a), leading to higher drift speed values. The modelled drift speed is closer to observations with $P^* = 5.5$ kN m^{-2} in June and July, $P^* = 27.5$ kN m^{-2} in May and from September to November, $P^* = 45$ kN m^{-2} from December to February and in April, $P^* = 100$ kN m^{-2} in March. Therefore, there is no single P^* value that provides a best fit to observed drift speed.

Figure 13 shows the drift-concentration and drift-thickness relationships for the model with different P^* values as well as observations in terms of mean seasonal cycle averaged over the period 1979-2013 and over the SCICEX box. All model simulations but one ($P^* = 5.5$ kN m^{-2}) provide coherent relationships with significant slopes at the 5 % level, i.e. a decreasing drift speed with increasing concentration and thickness as well as a hysteresis loop for the drift-thickness relationship. For the drift-concentration relationship (Fig. 13a), the $P^* = 45$ kN m^{-2} curve is closer to observations in terms of slope ratio ($s_A = 0.7$) and normalised distance ($\epsilon_A = 2.5\%$). For the drift-thickness relationship (Fig. 13b), the slope ratio is the highest with $P^* = 100$ kN m^{-2} ($s_h = 0.8$) and the normalised distance is the smallest with $P^* = 20$ kN m^{-2} ($\epsilon_h = 6\%$). It is also clearly apparent from Fig. 13b that a higher P^* parameter value leads to lower thickness and a higher amplitude of the seasonal cycle of drift speed.

4 Discussion

4.1 Novelties of the present study

The main novelty of the present study is the in-depth analysis of the interactions between Arctic sea ice drift and sea ice strength (concentration and thickness) via an extension of the work carried out by Olason and Notz (2014) and a series of model sensitivity experiments in which the sea ice strength is varied. Rampal et al. (2011) mention these interactions as an

important element of Arctic sea ice processes and other studies analyse interactions between some elements of the system (Spreen et al., 2011; Kwok et al., 2013; Langehaug et al., 2013; Olason and Notz, 2014), but none of these studies quantifies the magnitude of drift-strength interactions in detail. Here we address this issue using NEMO-LIM3.6 at $1°$ resolution with several process-based diagnostics and metrics as well as sensitivity experiments with different values of initial sea ice strength.

5   The drift-concentration and drift-thickness diagnostics and metrics used here are based on the work of Olason and Notz (2014). They analyse the interactions between the three variables using different observational datasets within the SCICEX box. On seasonal timescales, they find that sea ice concentration controls sea ice drift speed in summer (when concentration is relatively low) and sea ice thickness is the main driver in winter (when concentration is relatively high). In our analysis, we include model results and we also find that drift speed is anti-correlated to concentration during summer months in the

10   same SCICEX box (Fig. 8a). We also find that drift speed is anti-correlated to thickness not only during winter months but also during summer (with a clearer relationship for the observations compared to the model, Fig. 8b). In our study, we do not normalise sea ice drift speed by wind friction speed as in Olason and Notz (2014) because the same relationship is found with and without normalisation. In sum, we find that on seasonal timescales drift speed is controlled by both thickness and concentration.

15   There are some similarities between the results arising from our sensitivity experiments and the findings from Steele et al. (1997), which use a 40 km-resolution sea ice model based on Hibler (1979) over 7 model years. They explain that, as P^* decreases (for $P^* < 30\text{-}40\,\mathrm{kN\,m^{-2}}$), internal stress gradient decreases and mean ice motion increases (with ice nearly in free drift for $P^* = 5.5\,\mathrm{kN\,m^{-2}}$), which leads to higher ice thickness. However, for $P^* > 55\,\mathrm{kN\,m^{-2}}$, ice thickness slightly increases with increasing P^* in Steele et al. (1997) due to the progressive locking of sea ice (the ice motion ceases), providing an ice

20   thickness mainly determined by equilibrium thermodynamics. We do not observe this nonlinearity in our sensitivity experiments as ice thickness continues decreasing with increasing P^* for $P^* \geq 45\,\mathrm{kN\,m^{-2}}$ (Fig. 9a). Several reasons could explain this difference between Steele et al. (1997) and our study, including differences in model physics (e.g. ice thickness distribution included in our model), model parameters (e.g. grid resolution, time step), experimental setup (e.g. model years) and averaging domain. However, in our experiments, ice thickness from February to June is very similar between $P^* = 45\,\mathrm{kN\,m^{-2}}$ and $P^* = $

25   $100\,\mathrm{kN\,m^{-2}}$ (Fig. 9a) and deformation rates with $P^* = 100\,\mathrm{kN\,m^{-2}}$ are relatively high (Fig. 11a). Therefore, this nonlinearity may occur for $P^* > 100\,\mathrm{kN\,m^{-2}}$.

Our study can also be used to identify which P^* values yield results close to reference products (observations and reanalyses). Our findings suggest that the best match is strongly dependent upon the month of the year. For sea ice thickness, the amplitude of the modelled seasonal cycle is higher than the ones derived from submarine observations and PIOMAS renalysis,

30   so that all P^* values ranging from 5.5 to $100\,\mathrm{kN\,m^{-2}}$ could be used depending on the month (Fig. 9a). For drift speed, the highest values of P^* (45 and $100\,\mathrm{kN\,m^{-2}}$) better match observations in winter, and the lowest value ($5.5\,\mathrm{kN\,m^{-2}}$)) is more suitable in summer (Fig. 9b). In agreement with Massonnet et al. (2014), we do not recommend a specific value of P^*, since the optimal value for that parameter is dependent on many factors (resolution, atmospheric forcing, values chosen for other parameters, initial conditions, model). We still recommend excluding the lowest value ($P^* = 5.5\,\mathrm{kN\,m^{-2}}$) from the possibilities due

35   to a weaker representation of the drift-concentration and drift-thickness relationships (Fig. 13). This shows the limitations of

the parameterisation from Hibler (1979) and could support the use of new sea ice rheologies, such as the elasto-brittle rheology (Girard et al., 2011; Dansereau et al., 2016).

4.2 Complexity of drift-strength interactions

The potential positive feedback between sea ice drift and strength that is described in Rampal et al. (2011) proposes that an initial decrease in sea ice concentration or thickness leads to a decrease of sea ice strength and internal stress. This results in larger deformation and enhanced drift speed. According to Rampal et al. (2011), this would lead to an increased export of sea ice out of the Arctic Basin. This finally would lead to further decreases in sea ice concentration and thickness. However, observations do not show an increase in ice export (Döscher et al., 2014) while there is a clear decrease in concentration and thickness (Stroeve et al., 2012; Vaughan et al., 2013) and increase in drift speed (Spreen et al., 2011). Furthermore, our study shows that, even if this positive feedback exists, it is more complex than Rampal et al. (2011) suggest for two main reasons.

The first complication is the fact that a change in export of sea ice is not only a cause but also a consequence of changes in concentration and thickness. The volume export is the product of sea ice drift speed, concentration and thickness. Therefore, a decrease in concentration or thickness will both emphasize the positive feedback by increasing drift speed and the resulting export of sea ice, and reduce its magnitude by directly decreasing export of sea ice. This will balance the resulting sea ice export. We compute sea ice export at Fram Strait from sea ice drift speed, thickness (which takes into account concentration, since our thickness is the sea ice volume per area) and transect length at two different latitudes (76°N and 80°N) following Spreen et al. (2009). From 1979 to 2013, the volume flux modelled by NEMO-LIM3.6 decreases with a negative trend of 1.8 km^3 d^{-1} decade^{-1} in the control simulation (P^* = 20 kN m^{-2}) but interannual variations are very large, especially at the southern transect (76°N). Increasing ice strength (by increasing P^*) results in a decreasing volume flux at Fram Strait mainly due to the lower thickness. Therefore, in our model the direct effect of decreasing concentration and thickness is more important than the impact of increasing drift speed on the export at Fram Strait.

The second source of complexity is the fact that sea ice thickness decreases with higher ice strength (Section 3.3). If the drift-strength feedback dominated in our P^* experiments, ice thickness would be higher for higher ice strength (higher P^*), due to lower drift speed and export. However, ice thickness decreases with higher ice strength due to lower deformation (Figs. 9a and 11a). Thus, isolating the drift-strength feedback with a set of sensitivity experiments is difficult.

A previous study demonstrated the impact of increased ice strength using a coupled ice-ocean model to account for large-scale effects (Häkkinen and Mellor, 1992). They use both the classical Hibler parameterisation for ice strength as well as a square dependence of ice strength on thickness for first-year sea ice following Overland and Pease (1988) and compare both approaches. They show that increased ice strength leads to thicker ice, which is different from what we find in this study (increased strength leads to thinner ice). However, Häkkinen and Mellor (1992) do not use an ITD scheme, which may explain the difference with our results. Some sea ice models that include an ITD scheme use P scaling as $h^{3/2}$ since it is more physically realistic than P scaling as h (Rothrock, 1975). However, using such a scaling is less numerically stable (Lipscomb et al., 2007) and leads to poorer agreement with observations (Ungermann et al., 2017). According to Leppäranta (2011), the exact value of the thickness exponent remains an open question.

To test the impact of such a scaling on the resulting ice thickness and drift speed, we also performed sensitivity experiments in which we introduce an exponent λ in the ice strength equation (1), varying between 0.5 and 2 ($\lambda = 1$ corresponds to the original formulation of Hibler (1979)):

$$P = P^* h^\lambda \exp[-C(1-A)]. \tag{5}$$

5   These experiments are more complex than the P^* experiments since they introduce a nonlinear dependence between ice strength P and ice thickness h but they provide insight into the understanding of the impact of a change in the ice strength parameterisation. Overall, these experiments lead to similar conclusions as for the P^* experiments: higher λ leads to lower ice thickness, lower drift speed in winter and higher drift speed in summer, lower ice thickness heterogeneity, and a similar behaviour for drift-concentration and drift-thickness relationships.

10   An additional element that has not been studied here and could increase the complexity of the drift-strength interactions is the interaction between the ocean-sea ice system and the atmosphere. In this analysis, we use an ocean-sea ice model forced by atmospheric reanalysis. A full coupling with the atmosphere could provide different results regarding drift-strength interactions. For example, Juricke and Jung (2014) find that the implementation of a stochastic sea ice strength parameterisation leads to different responses in the coupled ECHAM6-FESOM model compared to the FESOM model forced by atmospheric fluxes 15   generated by the coupled model. In the uncoupled simulation, the Arctic sea ice volume increases compared to a reference run without parameterisation, while the volume remains largely unchanged in the coupled simulation. This suggests that a negative atmospheric feedback explains the differences between both coupled and uncoupled modes. Therefore, care needs to be taken when extrapolating results from forced simulations to coupled models. Specifically for our study, the effect of coupling on drift-strength interactions could be assessed by comparing our results to coupled simulations using NEMO-LIM3.6 (e.g. EC-Earth 20   in the framework of CMIP6).

4.3   Impact of domain choice

In this study, we compute spatial means both over the SCICEX box, roughly corresponding to the Central Arctic, and over a wider domain encompassing all grid cells north of $50°$N with a concentration threshold ($A \geq 0.15$). We prefer using the SCICEX box in our study because it produces much better agreement between the model and observations. The wider domain 25   includes the large model biases occurring in the vicinity of the ice front and of straits, e.g. model overestimation of drift speed at Fram Strait (Fig. 5).

   The use of the wider domain produces results for drift-concentration and drift-thickness relationships that clearly diverge compared to observations due to the inclusion of coastal grid cells that have high model biases. Computing mean concentration, thickness and drift speed over the Central Arctic (SCICEX box in our analysis) provides values that are much more consistent 30   with observations and more representative of Arctic conditions.

   Therefore, the comparison between our central and wide domains demonstrates the impact of domain choice, with generally better performance when using the central domain. A decomposition of the Arctic Ocean into sub-regions such as in Koenigk et al. (2016) would be a possible improvement compared to the use of a single wider domain.

4.4 How can this methodology help in future model intercomparisons?

The methodology proposed in this analysis, particularly the process-based diagnostics and metrics, can be used to assess the performance of other models against observational datasets, which will be an important component of SIMIP (Notz et al., 2016). It can be extended to models being forced by atmospheric reanalysis (such as the model used here) as well as fully coupled models, in order to provide a benchmark for further model intercomparison. In the framework of such a model intercomparison, the use of the process-based metrics that we developed (slope ratios and normalised distances) may be valuable for identifying which models fall within the observational range.

In this study, we only focus on one model resolution. Although some preliminary results show that a higher spatial resolution with the same model provides a higher sea ice thickness, there is a need for a deeper analysis of the impact of model resolution. The methodology proposed fits quite well into the framework of the EU Horizon 2020 PRIMAVERA project (https://www.primavera-h2020.eu/), which aims at evaluating the effect of high resolution in global climate models.

Finally, this process-based analysis provides an alternative to classic model evaluations that only look at sea ice extent and thickness. It systematically highlights the links between sea ice dynamic and thermodynamic processes. Evaluating new sea ice rheologies using this methodology will provide a stronger test of model performance.

5 Conclusions

This study first shows that the global ocean-sea ice NEMO-LIM3.6 model is able to reproduce the observed sea ice extent, concentration, thickness and drift speed reasonably well over the historical period (from 1979 to 2013). Monthly mean trends in concentration, thickness and drift speed are also in the observational range, except for the trend in drift speed during summer. We show that this model bias is linked to the removal of sea ice in the eastern Central Arctic rather than an actual decrease of drift speed.

The interactions between sea ice drift speed and strength are well represented through the relationships between drift speed and concentration on the one hand, and drift speed and thickness on the other hand. In particular, the increasing drift speed with lower concentration and thickness is reproduced by the model. The drift-thickness relationship is marked by a hysteresis loop: two drift speed values are possible for a given thickness depending on the season, with a higher sea ice drift speed during the melting season and a lower value during the growing season. When considering the relationships between the trends in drift speed, concentration and thickness, the spread between the model and observations is higher mainly due to too low summer trend in modelled drift speed.

Sensitivity experiments show that higher initial ice strength leads to lower ice thickness. This is due to lower deformation rates that prevents ice piling up, especially north of Greenland and the Canadian Archipelago. In the case of the highest strength experiment used here, net ice production is relatively low, which compensates for relatively high deformation rates. These experiments also show that no single value of P^* is the best option for reproducing the observed drift speed and thickness, but the best option depends on the variable and on the month of the year. We suggest that other rheologies might be more appropriate.

Finally, this study shows that the interactions between sea ice dynamics and state are complex and cannot be summarised by a simple feedback loop. The diagnostics and metrics proposed in this study that relate drift speed to concentration and thickness are necessary conditions for representing the drift-strength interactions, but they are not sufficient. Sensitivity experiments in which sea ice strength is varied are also essential for gaining insight into these interactions. While NEMO-LIM3.6 correctly represents the drift-concentration and drift-thickness relationships, sensitivity experiments show that processes other than the drift-strength feedback are more important in driving sea ice thickness and drift speed responses. In this analysis, we use one resolution of one model with an atmospherically forced mode. A multi-model assessment using different model resolutions, e.g. in the framework of the EU Horizon 2020 PRIMAVERA project, will provide further insight into the interactions between sea ice dynamics and state.

6 Code availability

All codes for computing and plotting the results of this article are written in Python programming language and are available upon request.

Author contributions. DD, FM and TF designed the experimental study. FM and AB performed the model simulations. DD collected the observational datasets, developed the diagnostics and metrics, analysed the results and produced the figures. NFT and OL provided substantial feedback to the analysis. DD prepared the manuscript with contributions from all co-authors.

Competing interests. The authors declare that they have no conflict of interest.

Acknowledgements. DD and AB work on the PRIMAVERA project (PRocess-based climate sIMulation: AdVances in high-resolution modelling and European climate Risk Assessment), which is funded by the European Commission's Horizon 2020 programme, grant agreement no. 641727. FM is funded by the Belgian Fonds National de la Recherche Scientifique (FNRS) and was funded by the Ministerio de Economía, Industria y Competitividad (MINECO). NFT is supported by the Canadian Sea Ice and Snow Evolution (CanSISE) Network. OL is a research assistant within the Belgian FNRS. The present research benefited from computational resources made available on the Tier-1 supercomputer of the Fédération Wallonie-Bruxelles, infrastructure funded by the Walloon Region under the grant agreement n°1117545. Computational resources have also been provided by the Consortium des Équipements de Calcul Intensif (CÉCI), funded by the Fonds de la Recherche Scientifique de Belgique (F.R.S.-FNRS) under grant no. 2.5020.11. We would like to thank H. Goosse, M. Vancoppenolle, J. Raulier and V. Dansereau for their very helpful comments regarding this study. We also acknowledge P.-Y. Barriat for his help in using computing resources at UCL and D. François for his advice in improving Python scripts. Finally, we thank the editor D. Notz and the two anonymous reviewers.

References

Comiso, J.: Bootstrap Sea Ice Concentrations from Nimbus-7 SMMR and DMSP SSM/I-SSMIS, Version 2, doi:10.5067/J6JQLS9EJ5HU, http://nsidc.org/data/nsidc-0079#, 2015.

Comiso, J. C.: Characteristics of Arctic winter sea ice from satellite multispectral microwave observations, Journal of Geophysical Research, 91, 975–994, 1986.

Comiso, J. C., Cavalieri, D. J., Parkinson, C. L., and Gloersen, P.: Passive microwave algorithms for sea ice concentration: A comparison of two techniques, Remote Sensing of Environment, 60, 357–384, 1997.

Dansereau, V., Weiss, J., Saramito, P., and Lattes, P.: A Maxwell elasto-brittle rheology for sea ice modelling, The Cryosphere, 10, 1339–1359, doi:10.5194/tc-10-1339-2016, 2016.

Döscher, R., Vihma, T., and Maksimovich, E.: Recent advances in understanding the Arctic climate system state and change from a sea ice perspective: a review, Amospheric Chemistry and Physics, 14, 13 571–13 600, doi:10.5194/acp-14-13571-2014, 2014.

Dupont, F., Higginson, S., Bourdallé-Badie, R., Lu, Y., Roy, F., Smith, G. C., Lemieux, J.-F., Garric, G., and Davidson, F.: A high-resolution ocean and sea-ice modelling system for the Arctic and North Atlantic oceans, Geoscientific Model Development, 8, 1577–1594, doi:10.5194/gmd-8-1577-2015, 2015.

Dussin, R., Barnier, B., Brodeau, L., and Molines, J. M.: The making of the Drakkar Forcing Set DFS5, Tech. rep., Multiscale Ocean Modelling Team, Laboratoire de Glaciologie et Géophysique de l'Environnement, Grenoble, France, https://www.drakkar-ocean.eu/forcing-the-ocean, 2016.

EUMETSAT OSI SAF: Global sea ice concentration reprocessing dataset 1978-2015 (v1.2), http://www.osi-saf.org/, 2015a.

EUMETSAT OSI SAF: Low resolution sea ice drift product, http://www.osi-saf.org/, 2015b.

Feltham, D. L.: Sea Ice Rheology, Annu. Rev. Fluid Mech., 40, 91–112, doi:10.1146/annurev.fluid.40.111406.102151, 2008.

Gimbert, F., Jourdain, N. C., Marsan, D., Weiss, J., and Barnier, B.: Recent mechanical weakening of the Arctic sea ice cover as revealed from larger inertial oscillations, Geophysical Research Letters, 117, C00J12, doi:10.1029/2011JC007633, 2012.

Girard, L., Bouillon, S., Weiss, J., Amitrano, D., Fichefet, T., and Legat, V.: A new modeling framework for sea-ice mechanics based on elasto-brittle rheology, Annals of Glaciology, 52(57), 123–132, 2011.

Haarsma, R. J., Roberts, M. J., Vidale, P. L., Senior, C. A., Bellucci, A., Bao, Q., Chang, P., Corti, S., Fuckar, N. S., Guemas, V., von Hardenberg, J., Hazeleger, W., Kodama, C., Koenigk, T., Leung, L. R., Lu, J., Luo, J.-J., Mao, J., Mizielinski, M. S., Mizuta, R., Nobre, P., Satoh, M., Scoccimarro, E., Semmler, T., Small, J., and von Storch, J.-S.: High Resolution Model Intercomparison Project (HighResMIP v1.0) for CMIP6, Geoscientific Model Development, 9, 4185–4208, doi:10.5194/gmd-9-4185-2016, 2016.

Häkkinen, S. and Mellor, G. L.: Modeling the seasonal variability of a coupled Arctic ice-ocean system, Journal of Geophysical Research, 97, 20 285–20 304, doi:10.1029/92JC02037, 1992.

Häkkinen, S., Proshutinsky, A., and Ashik, I.: Sea ice drift in the Arctic since the 1950s, Geophysical Research Letters, 35, L19 704, doi:10.1029/2008GL034791, 2008.

Hibler, W. D.: A Dynamic Thermodynamic Sea Ice Model, Journal of Physical Oceanography, 9, 815–846, 1979.

Hibler, W. D. and Walsh, J. E.: On modeling seasonal and interannual fluctuations of Arctic sea ice, Journal of Physical Oceanography, 12, 1514–1523, 1982.

Ivanova, N., Pedersen, L. T., Tonboe, R. T., Kern, S., Heygster, G., Lavergne, T., Sørensen, A., Saldo, R., Dybkjær, G., Brucker, L., and Shokr, M.: Inter-comparison and evaluation of sea ice algorithms: towards further identification of challenges and optimal approach using passive microwave observations, The Cryosphere, 9, 1797–1817, doi:10.5194/tc-9-1797-2015, 2015.

Juricke, S. and Jung, T.: Influence of stochastic sea ice parametrization on climate and the role of atmosphere-sea ice-ocean interaction, Philos. Trans. A Math. Phys. Eng. Sci., 28, 372, doi:10.1098/rsta.2013.0283, 2014.

Juricke, S., Lemke, P., Timmerman, R., and Rackow, T.: Effects of stochastic ice strength perturbation on Arctic finite element sea ice modeling, Journal of Climate, 26, 3785–3802, doi:10.1175/JCLI-D-12-00388.1, 2013.

Koenigk, T., Caian, M., Nikulin, G., and Schimanke, S.: Regional Arctic sea ice variations as predictor for winter climate conditions, Climate Dynamics, 46, 317–337, doi:10.1007/s00382-015-2586-1, 2016.

Kreyscher, M., Harder, M., and Lemke, P.: First results of the Sea-Ice Model Intercomparison Project (SIMIP), Annals of Glaciology, 25, 8–11, doi:10.1017/S0260305500013719, 1997.

Krumpen, T., Gerdes, R., Haas, C., Hendrickx, S., Herber, A., Selyuzhenok, V., Smedsrud, L., and Spreen, G.: Recent summer sea ice thickness surveys in Fram Strait and associated ice volume fluxes, The Cryosphere, pp. 523–534, doi:10.5194/tc-10-523-2016, 2016.

Kwok, R.: Outflow of Arctic Ocean Sea Ice into the Greenland and Barents Seas: 1979–2007, Journal of Climate, 22, 2438–2457, doi:10.1175/2008JCLI2819.1, 2009.

Kwok, R., Cunningham, G. F., Wensnahan, M., Rigor, I., Zwally, H. J., and Yi, D.: Thinning and volume loss of the Arctic Ocean sea ice cover: 2003–2008, Journal of Geophysical Research, 114, 2009.

Kwok, R., Spreen, G., and Pang, S.: Arctic sea ice circulation and drift speed: Decadal trends and ocean currents, Journal of Geophysical Research, 118, 2408–2425, doi:10.1002/jgrc.20191, 2013.

Langehaug, H., Geyer, F., Smedsrud, L., and Gao, Y.: Arctic sea ice decline and ice export in the CMIP5 historical simulations, Ocean Modelling, 71, 114–126, 2013.

Large, W. G. and Yeager, S. G.: The global climatology of an interannually varying air–sea flux data set, Climate Dynamics, 33, 341–364, doi:10.1007/s00382-008-0441-3, 2009.

Lavergne, T., Eastwood, S., Teffah, Z., Schyberg, H., and Breivik, L.-A.: Sea ice motion from low-resolution satellite sensors: An alternative method and its evaluation in the Arctic, Journal of Geophysical Research, 115, C10 032, doi:10.1029/2009JC005958, 2010.

Leppäranta, M.: The drift of sea ice (Second Edition), Springer, 2011.

Lindsay, R. and Schweiger, A.: Arctic sea ice thickness loss determined using subsurface, aircraft, and satellite observations, The Cryosphere, 9, 269–283, doi:10.5194/tc-9-269-2015, 2015.

Lipscomb, W. H., Hunke, E. C., Maslowski, W., and Jakacki, J.: Ridging, strength, and stability in high-resolution sea ice models, Journal of Geophysical Research, 112, doi:10.1029/2005JC003355, 2007.

Madec, G.: NEMO ocean engine: Note du Pôle de modélisation de l'Institut Pierre-Simon Laplace No 27, http://www.nemo-ocean.eu/About-NEMO/Reference-manuals, 2016.

Massonnet, F., Goosse, H., Fichefet, T., and Counillon, F.: Calibration of sea ice dynamic parameters in an ocean-sea ice model using an ensemble Kalman filter, Journal of Geophysical Research, 119, 4168–4184, doi:10.1002/2013JC009705, 2014.

Massonnet, F., Bellprat, O., Guemas, V., and Doblas-Reyes, F. J.: Using climate models to estimate the quality of global observational data sets, Science, 354, 452–455, doi:10.1126/science.aaf6369, 2016.

Notz, D.: Sea-ice extent and its trend provide limited metrics of model performance, The Cryosphere, 8, 229–243, doi:10.5194/tc-8-229-2014, http://www.the-cryosphere.net/8/229/2014/, 2014.

Notz, D.: How well must climate models agree with observations?, Philosophical Transactions of the Royal Society of London, Series A: Mathematical and Physical Sciences, 373, doi:10.1098/rsta.2014.0164, 2015.

Notz, D., Jahn, A., Holland, M., Hunke, E., Massonnet, F., Stroeve, J., Tremblay, B., and Vancoppenolle, M.: The CMIP6 Sea-Ice Model Intercomparison Project (SIMIP): understanding sea ice through climate-model simulations, Geoscientific Model Development, 9, 3427–3446, doi:10.5194/gmd-9-3427-2016, 2016.

Olason, E. and Notz, D.: Drivers of variability in Arctic sea-ice drift speed, Journal of Geophysical Research, 119, 5755–5775, doi:10.1002/2014JC009897, 2014.

Overland, J. E. and Pease, C. H.: Modeling ice dynamics of coastal seas, Journal of Geophysical Research, 93, 15 619–15 637, doi:10.1029/JC093iC12p15619, 1988.

Polyakov, D. V., Walsh, J. E., and Kwok, R.: Recent changes of Arctic multiyear sea ice coverage and the likely causes, Bulletin of American Meteorological Society, 93, 145–151, doi:10.1175/BAMS-D-11-00070.1, 2012.

Rampal, P., Weiss, J., Marsan, D., and Bourgoin, M.: Arctic sea ice velocity field: General circulation and turbulent-like fluctuations, Journal of Geophysical Research, 114, C10 014, doi:10.1029/2008JC005227, 2009.

Rampal, P., Weiss, J., Dubois, C., and Campin, J.-M.: IPCC climate models do not capture Arctic sea ice drift acceleration: Consequences in terms of projected sea ice thinning and decline, Journal of Geophysical Research, 116, C00D07, doi:10.1029/2011JC007110, 2011.

Rothrock, D. A.: The energetics of the plastic deformation of pack ice by ridging, Journal of Geophysical Research, 80, 4514–4519, doi:10.1029/JC080i033p04514, 1975.

Rothrock, D. A. and Wensnahan, M.: The accuracy of sea-ice drafts measured from U.S. Navy submarines, Journal of Atmospheric and Ocean Technology, 24, 1936–1949, doi:10.1175/JTECH2097.1, 2007.

Rothrock, D. A., Percival, D. B., and Wensnahan, M.: The decline in Arctic sea-ice thickness: Separating the spatial, annual, and interannual variability in a quarter century of submarine data, Journal of Geophysical Research, 113, C05 003, doi:10.1029/2007JC004252, 2008.

Rousset, C., Vancoppenolle, M., Madec, G., Fichefet, T., Flavoni, S., Barthélemy, A., Benshila, R., Chanut, J., Levy, C., Masson, S., and Vivier, F.: The Louvain-La-Neuve sea ice model LIM3.6: global and regional capabilities, Geoscientific Model Development, 8, 2991–3005, doi:10.5194/gmd-8-2991-2015, 2015.

Schweiger, A., Lindsay, R., Zhang, J., Steele, M., Stern, H., and Kwok, R.: Uncertainty in modeled Arctic sea ice volume, Journal of Geophysical Research, 116, C00D06, doi:10.1029/2011JC007084, 2011.

Smedsrud, L. H., Halvorsen, M. H., Stroeve, J. C., Zhang, R., and Kloster, K.: Fram Strait sea ice export variability and September Arctic sea ice extent over the last 80 years, The Cryosphere, 11, 65–79, doi:10.5194/tc-11-65-2017, 2016.

Smith, D.: Extraction of winter total sea ice concentration in the Greenland and Barents Seas from SSM/I data, International Journal of Remote Sensing, 17, 2625–2646, 1996.

Spreen, G., Kern, S., Stammer, D., and Hansen, E.: Fram Strait sea ice volume export estimated between 2003 and 2008 from satellite data, Geophysical Research Letters, 36, L19 502, doi:10.1029/2009GL039591, 2009.

Spreen, G., Kwok, R., and Menemenlis, D.: Trends in Arctic sea ice drift and role of wind forcing: 1992-2009, Geophysical Research Letters, 38, L19 501, doi:10.1029/2011GL048970, 2011.

Spreen, G., Kwok, R., Menemenlis, D., and Nguyen, A. T.: Sea-ice deformation in a coupled ocean–sea-ice model and in satellite remote sensing data, The Cryosphere, 11, 1553–1573, doi:10.5194/tc-11-1553-2017, 2017.

Steele, M., Zhang, J., Rothrock, D., and Stern, H.: The force balance of sea ice in a numerical model of the Arctic Ocean, Journal of Geophysical Research: Oceans, 102, 21 061–21 079, doi:10.1029/97JC01454, 1997.

Stroeve, J., Barrett, A., Serreze, M., and Schweiger, A.: Using records from submarine, aircraft and satellites to evaluate climate model simulations of Arctic sea ice thickness, The Cryosphere, 8, 1839–1854, doi:10.5194/tc-8-1839-2014, 2014.

Stroeve, J. C., Serreze, M. C., Holland, M. M., Kay, J. E., Malanik, J., and Barrett, A. P.: The Arctic's rapidly shrinking sea ice cover: a research synthesis, Climatic Change, 110, 1005–1027, doi:10.1007/s10584-011-0101-1, 2012.

5   Sumata, H., Lavergne, T., Girard-Ardhuin, F., Kimura, N., Tschudi, M. A., Kauker, F., Karcher, M., and Gerde, R.: An intercomparison of Arctic ice drift products to deduce uncertainty estimates, Journal of Geophysical Research, 119, 4887–4921, doi:10.1002/2013JC009724, 2014.

Szanyi, S., Lukovich, J. V., Barber, D. G., and Haller, G.: Persistent artifacts in the NSIDC ice motion data set and their implications for analysis, Geophysical Research Letters, pp. 10 800–10 807, doi:10.1002/2016GL069799, 2016.

10 Tandon, N. F., Kushner, P. J., Docquier, D., Wettstein, J. J., and Li, C.: Reassessing the role of sea ice drift in Arctic sea ice loss, submitted.

Tremblay, L.-B. and Hakakian, M.: Estimating the Sea Ice Compressive Strength from Satellite-Derived Sea Ice Drift and NCEP Reanalysis Data*, J. Phys. Oceanogr., 36, 2165–2172, doi:10.1175/JPO2954.1, http://dx.doi.org/10.1175/JPO2954.1, 2006.

Tschudi, M., Fowler, C., Maslanik, J., Stewart, J. S., and Meier, W.: Polar Pathfinder Daily 25 km EASE-Grid Sea Ice Motion Vectors, Version 3 [IABP buoys], doi:10.5067/O57VAIT2AYYY, http://nsidc.org/data/NSIDC-0116/versions/3, 2016.

15 Ungermann, M., Tremblay, L. B., Martin, T., and Losch, M.: Impact of the ice strength formulation on the performance of a sea ice thickness distribution model in the Arctic, Journal of Geophysical Research, 122, 2090–2107, doi:10.1002/2016JC012128, 2017.

Vancoppenolle, M., Fichefet, T., Goosse, H., Bouillon, S., Madec, G., and Morales Maqueda, M. A.: Simulating the mass balance and salinity of Arctic and Antarctic sea ice. 1. Model description and validation, Ocean Modelling, 27, 33–53, doi:10.1016/j.ocemod.2008.10.005, 2009.

20 Vaughan, D., Comiso, J., Allison, I., Carrasco, J., Kaser, G., Kwok, R., Mote, P., Murray, T., Paul, F., Ren, J., Rignot, E., Solomina, O., Steffen, K., and Zhang, T.: Observations: Cryosphere. In Climate Change 2013: The Physical Science Basis. Contribution of Working Group I to the Fifth Assessment Report of the Intergovernmental Panel on Climate Change [Stocker, T. F., D. Qin, G.-K. Plattner, M. Tignor, S. K. Allen, J. Boschung, A. Nauels, Y. Xia, V. Bex and P. M. Midgley (eds.)]., Cambridge University Press, Cambridge, United Kingdom and New York, NY, USA, 2013.

25 Vihma, T., Tisler, P., and Uotila, P.: Atmospheric forcing on the drift of Arctic sea ice in 1989–2009, Geophysical Research Letters, 39, L02 501, doi:10.1029/2011GL050118, 2012.

Zhang, J. and Rothrock, D. A.: Modeling global sea Iie with a thickness and enthalpy distribution model in generalized curvilinear coordinates, Monthly Weather Review, 131, 845–861, 2003.

Zygmuntowska, M., Rampal, P., Ivanova, N., and Smedsrud, L. H.: Uncertainties in Arctic sea ice thickness and volume: new estimates and 30   implications for trends, The Cryosphere, 8, 705–720, doi:10.5194/tc-8-705-2014, 2014.
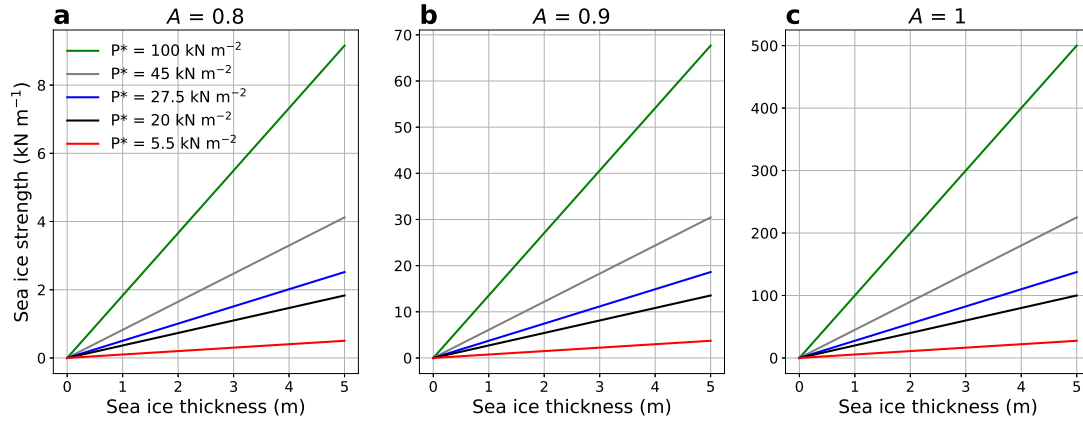
Figure 1. Sea ice strength as a function of sea ice thickness computed from Eq. (1) (Hibler, 1979) for five given values of P^* corresponding to the five sensitivity experiments. The three panels correspond to three different values of sea ice concentration: (a) $A = 0.8$, (b) $A = 0.9$, (c) $A = 1$. Note that the y axes are different in the three panels.
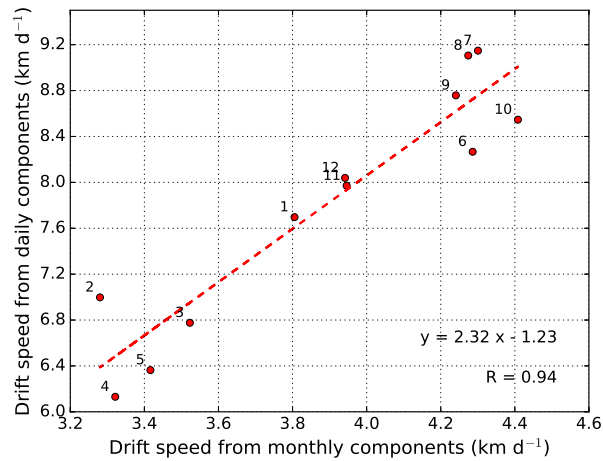
Figure 2. Scatter plot of modelled (NEMO-LIM3.6) monthly mean sea ice drift speed computed from daily components against drift speed based on monthly components. Data are temporally averaged over the period 1979-2013 and spatially averaged over the SCICEX box. Numbers denote months. The dashed line represents the linear regression. The equation of the linear regression and the Pearson correlation coefficient between both variables are shown in the lower right corner.
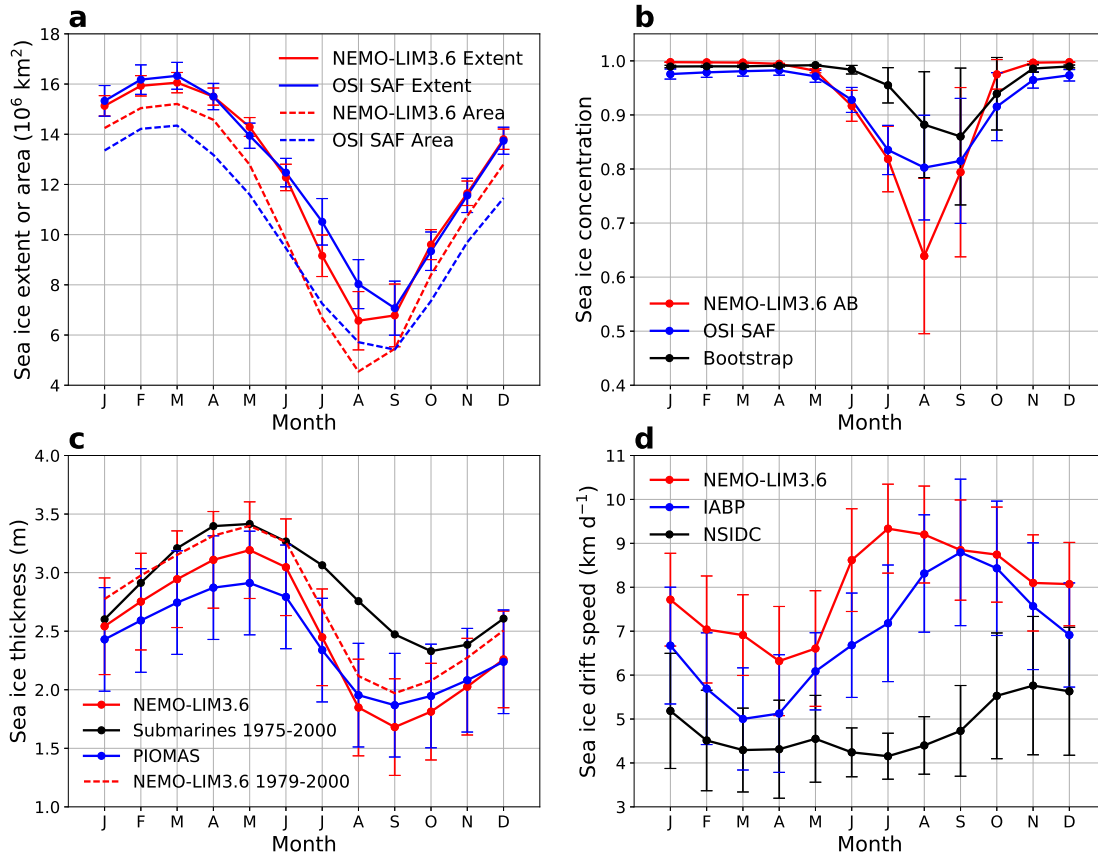
Figure 3. Modelled (NEMO-LIM3.6) and observed monthly mean seasonal cycles of Arctic sea ice (a) extent (total area of grid cells where concentration is higher than 0.15) and area, (b) concentration, (c) thickness (sea ice volume per area) and (d) drift speed averaged over the period 1979-2013 (except for submarine observations that span 1975-2000). The spatial mean over the SCICEX box is shown in (b), (c) and (d). Sources for observations and reanalysis: OSI SAF satellite data for extent and concentration, Bootstrap satellite data for concentration, submarines and PIOMAS reanalysis for thickness, IABP buoys and NSIDC (Tschudi et al., 2016) for drift speed. Error bars show the temporal standard deviation of monthly values. In panel (c), the model seasonal cycle is also computed over 1979-2000 to allow for more direct comparison with submarine observations.
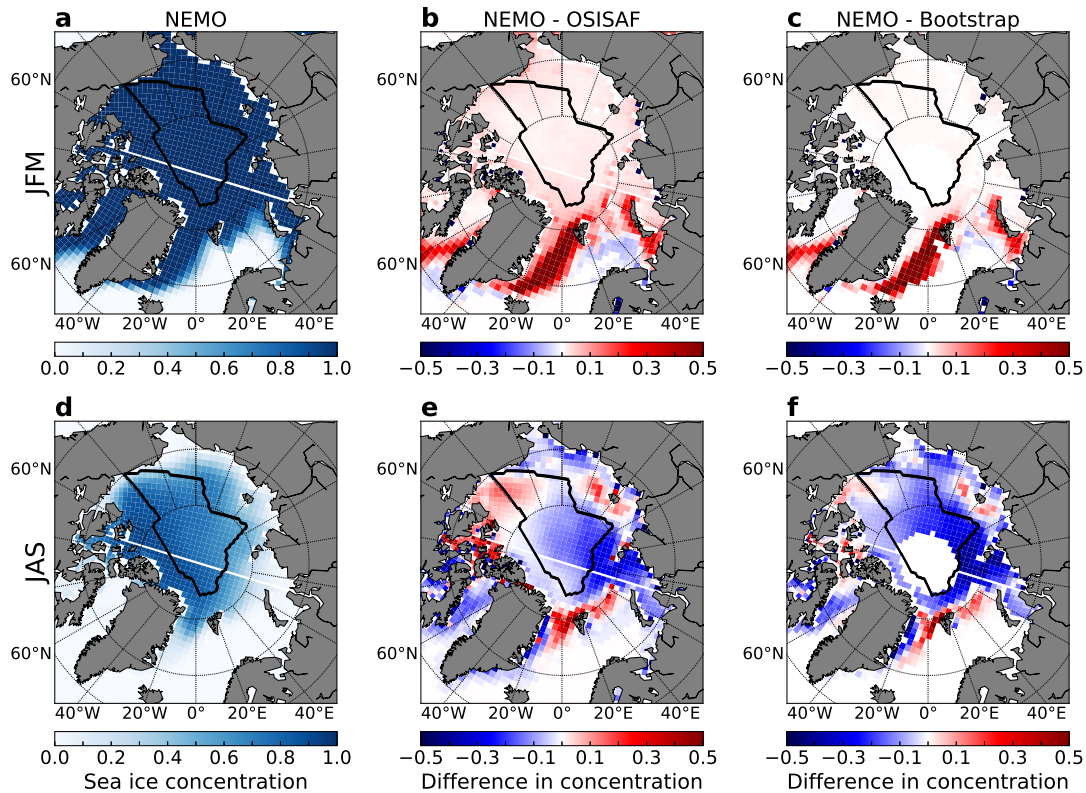
Figure 4. (a) Modelled (NEMO-LIM3.6) mean Arctic sea ice concentration averaged over the winter months (JFM, i.e. January-February-March) of the period 1979-2013. (b) Difference in concentration between NEMO-LIM3.6 and OSI SAF averaged over the winter months of the period 1979-2013. (c) Difference in concentration between NEMO-LIM3.6 and Bootstrap averaged over the winter months of the period 1979-2013. (d), (e), (f) Same as (a), (b), (c) respectively for the summer months (JAS, i.e. July-August-September). The black polygon marks the SCICEX box.
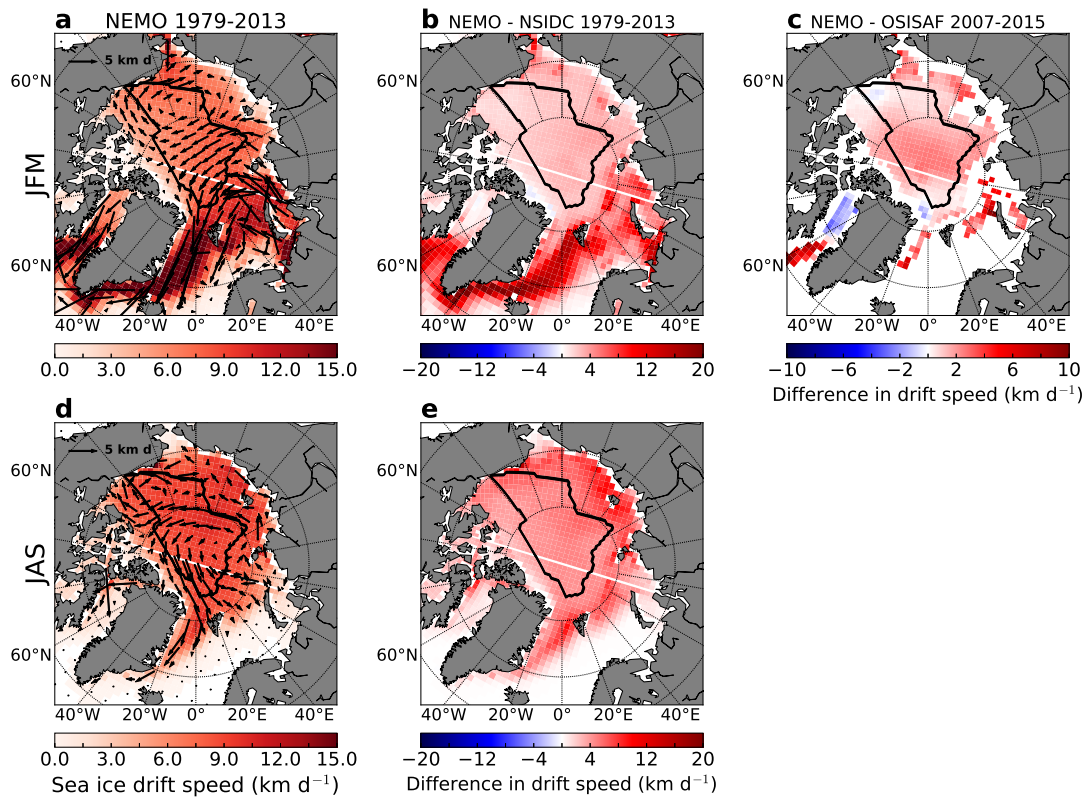
Figure 5. (a) Modelled (NEMO-LIM3.6) mean Arctic sea ice drift speed averaged over the winter months (JFM, i.e. January-February-March) of the period 1979-2013. (b) Difference in drift speed between NEMO-LIM3.6 and the NSIDC dataset (Tschudi et al., 2016) averaged over the winter months of the period 1979-2013. (c) Difference in drift speed between NEMO-LIM3.6 and OSI SAF averaged over the winter months of the period 2007-2015. (d), (e) Same as (a), (b) respectively for the summer months (JAS, i.e. July-August-September). OSI SAF drift data are not available in summer. The black polygon marks the SCICEX box.
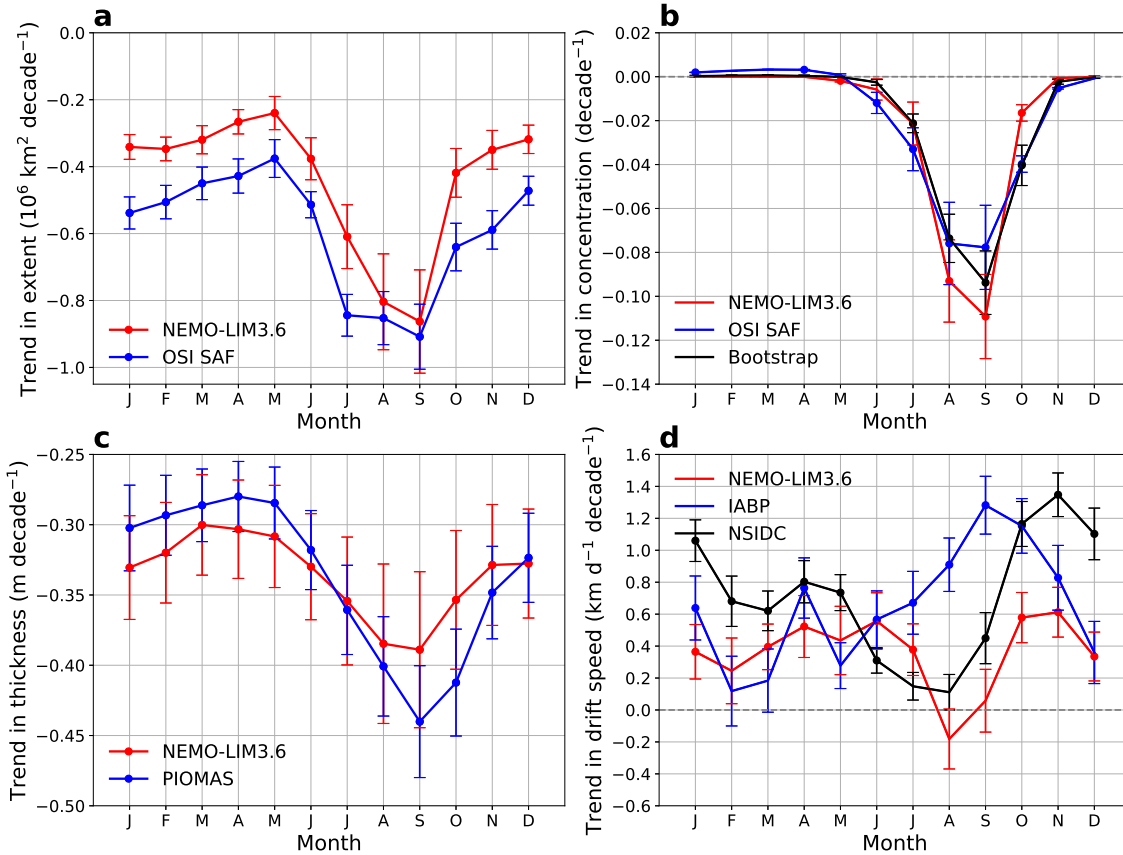
Figure 6. Modelled (NEMO-LIM3.6) and observed monthly mean seasonal cycles of trends in Arctic sea ice (a) extent, (b) concentration, (c) thickness and (d) drift speed averaged over the period 1979-2013. The spatial mean over the SCICEX box is shown in (b), (c) and (d). A dot is shown for monthly trends that are significant at the 5% level. Sources for observations and reanalysis: OSI SAF satellite data for extent and concentration, Bootstrap satellite data for concentration, PIOMAS reanalysis for thickness, IABP buoys and NSIDC (Tschudi et al., 2016) for drift speed. Error bars show the temporal standard deviation of monthly values.
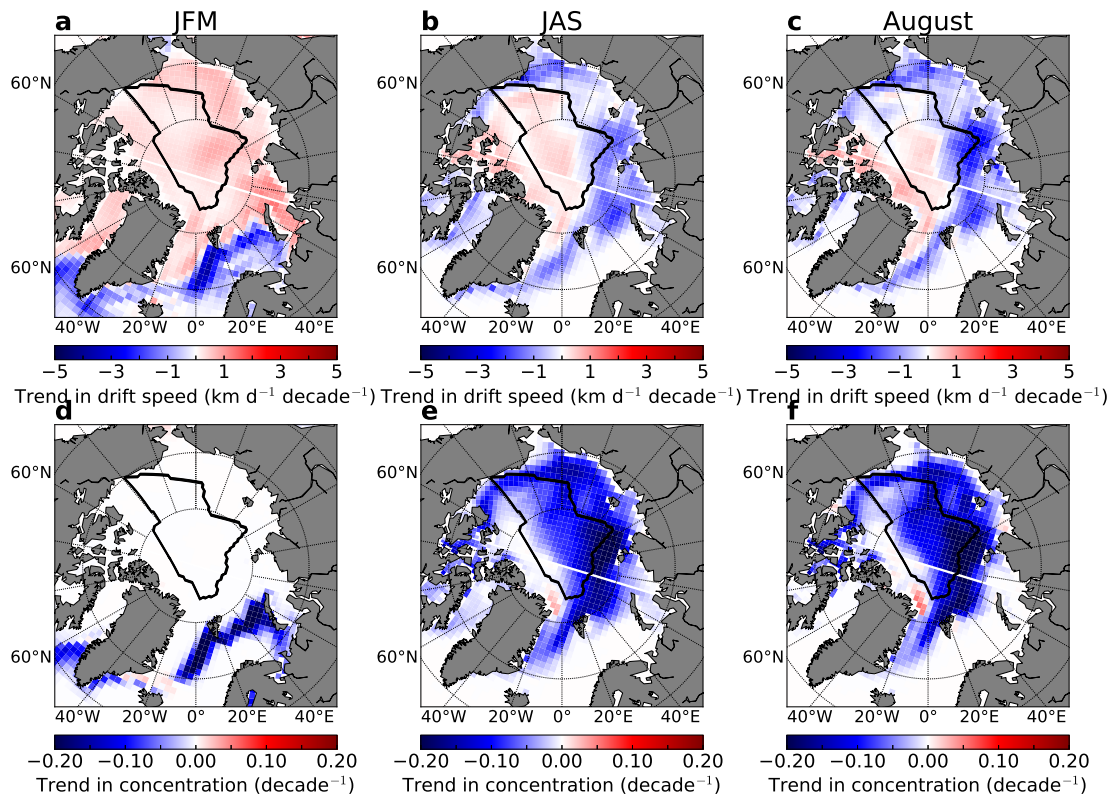
Figure 7. (a) Modelled (NEMO-LIM3.6) mean trend in Arctic sea ice drift speed averaged over the winter months (JFM, i.e. January-February-March) of the period 1979-2013. (b) Same as (a) for the summer months (JAS, i.e. July-August-September). (c) Same as (a) for August only. (d), (e), (f) Same as (a), (b), (c) respectively for sea ice concentration. The black polygon marks the SCICEX box.
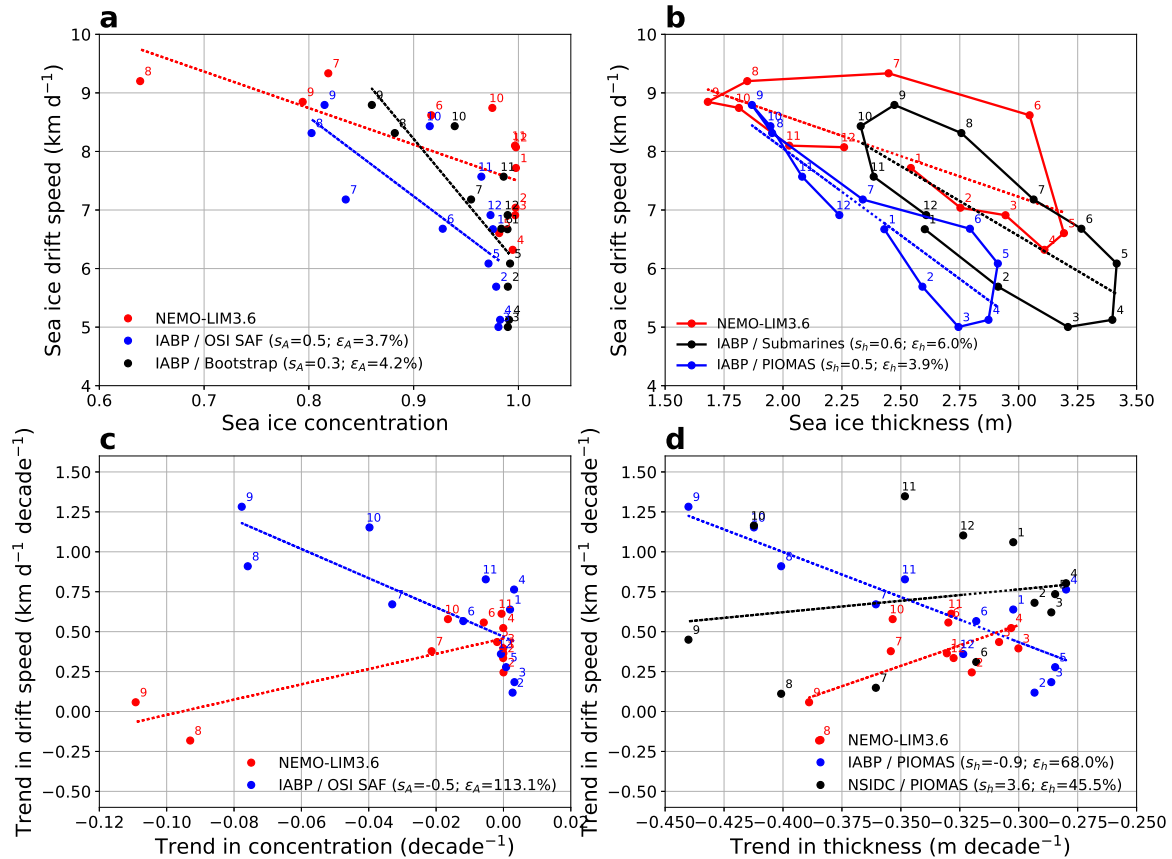
Figure 8. Scatter plots of modelled (NEMO-LIM3.6) and observed monthly mean sea ice drift speed against (a) concentration and (b) thickness temporally averaged over the period 1979-2013 (except for submarine observations that span 1975-2000) and spatially averaged over the SCICEX box. (c), (d) Same as (a), (b) for trends. Numbers denote months. Dotted lines show linear regressions. Sources for observations and reanalysis: IABP and NSIDC (Tschudi et al., 2016) for drift speed, OSI SAF and Boostrap for concentration, submarines and PIOMAS for thickness. Slope ratios and normalised distances between NEMO-LIM3.6 and the different observation datasets are shown in brackets in the legends.
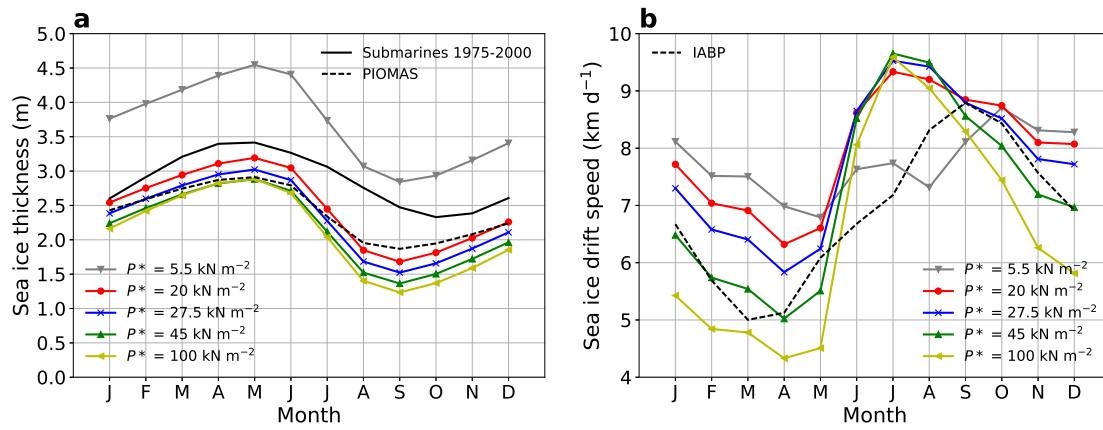
Figure 9. Modelled (NEMO-LIM3.6) monthly mean seasonal cycles of sea ice (a) thickness and (b) drift speed temporally averaged over the period 1979-2013 and spatially averaged over the SCICEX box for five different P^* values (see Eq. (1)). Observations and reanalysis are represented as black lines (submarine observations, spanning 1975-2000, and PIOMAS for thickness in (a) and IABP for drift speed in (b)).
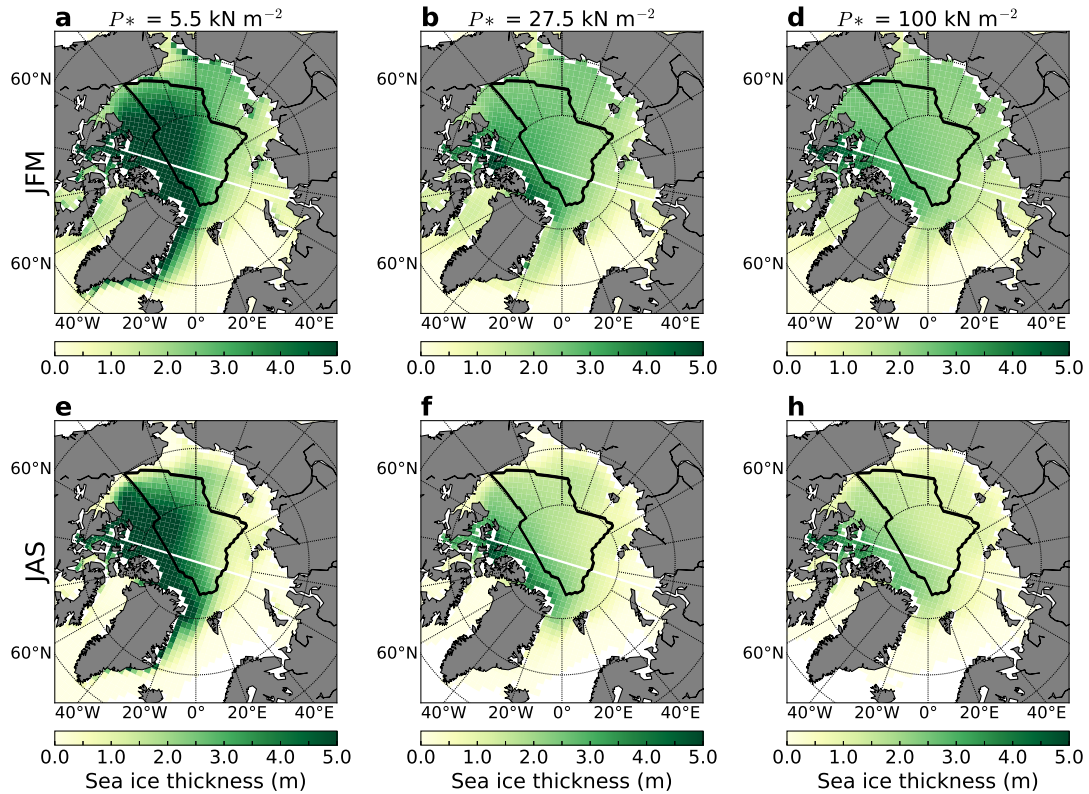
Figure 10. Modelled (NEMO-LIM3.6) mean Arctic sea ice thickness averaged over the winter months (JFM, i.e. January-February-March) of the period 1979-2013 for (a) $P^* = 5.5$ kN m^{-2}, (b) $P^* = 27.5$ kN m^{-2}, (c) $P^* = 100$ kN m^{-2}. (e), (f), (g) Same as (a), (b), (c) respectively for the summer months (JAS, i.e. July-August-September). The black polygon marks the SCICEX box.
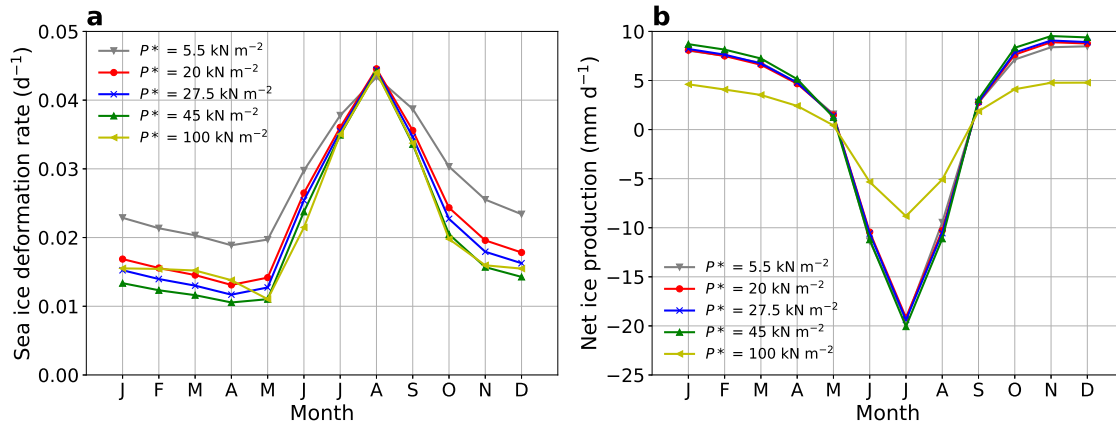
Figure 11. Modelled (NEMO-LIM3.6) monthly mean seasonal cycles of (a) sea ice deformation rate and (b) net ice production temporally averaged over the period 1979-2013 and spatially averaged over the SCICEX box for five different P^* values.
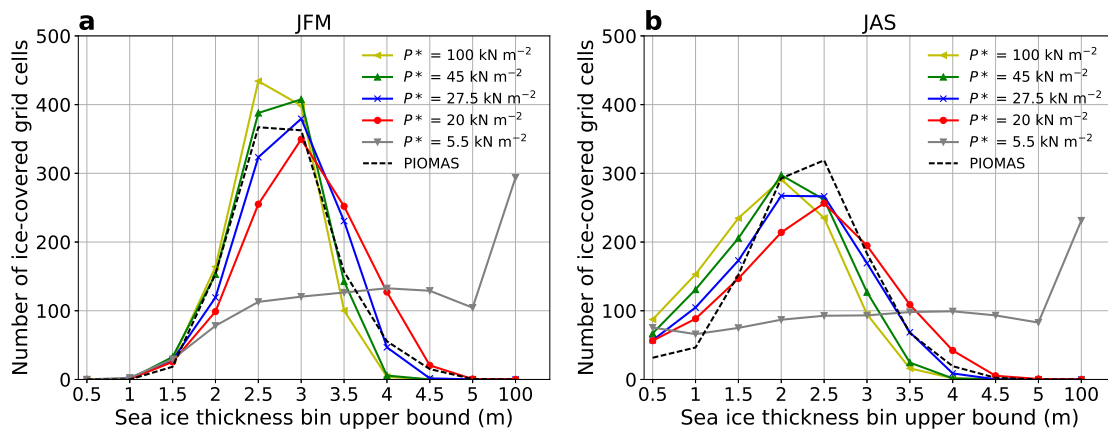
Figure 12. Number of ice-covered grid cells in each thickness bin temporally averaged over 1979-2013 and spatially averaged over the SCICEX box for both (a) winter (JFM, i.e. January-February-March) and (b) summer (JAS, i.e. July-August-September). Results are shown for NEMO-LIM3.6 (five different $P*$ values) and for PIOMAS reanalysis interpolated onto the eORCA1 grid. The x axis shows the upper bound of each thickness bin.
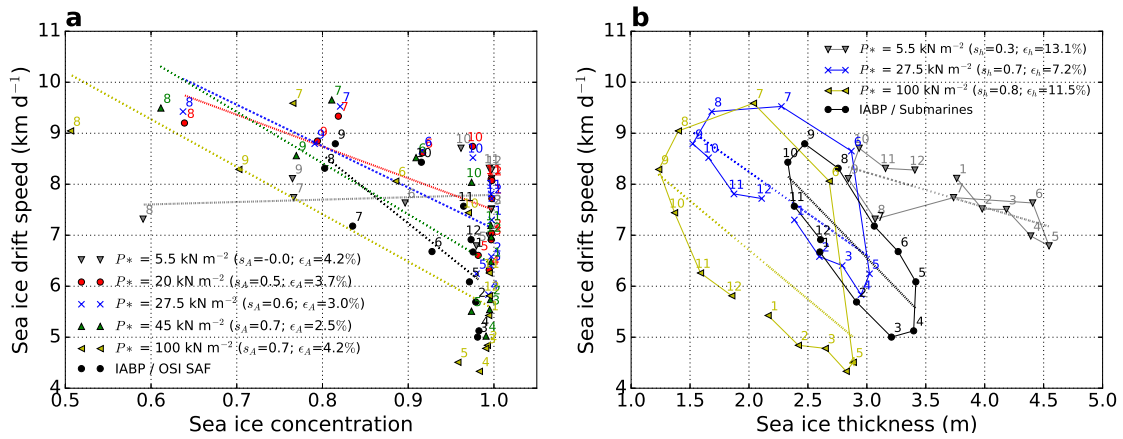
Figure 13. Scatter plots of modelled (NEMO-LIM3.6) monthly mean sea ice drift speed against sea ice (a) concentration and (b) thickness temporally averaged over the period 1979-2013 and spatially averaged over the SCICEX box for the different P^* values (only three values in (b) for readability). Numbers denote months. Observations and reanalysis are represented in black. Dotted lines show linear regressions. Slope ratios and normalised distances between NEMO-LIM3.6 and the different observation datasets are shown in brackets in the legend.

Table 1. Summary of published literature providing observational drift speed trend and its cause, as well as area and volume export of sea ice at Fram Strait.

Reference	Drift speed	Cause of drift increase	Area export	Volume export
Häkkinen et al. (2008)	1950-2006: significant positive trend	Wind		
Spreen et al. (2009)				1990-2008: no significant change
Kwok (2009)			1979-2007: no significant trend	
Rampal et al. (2009)	1979-2007: +17% decade^{-1} in winter +8.5% decade^{-1} in summer	Ice strength		
Spreen et al. (2011)	1992-2009: +10.6% decade^{-1}	Ice strength (first) Wind (second)		
Gimbert et al. (2012)		Ice strength		
Polyakov et al. (2012)			1979-1995: increase	
Vihma et al. (2012)	1989-2009: increase	Ice strength (first) Wind (second)		
Kwok et al. (2013)	1982-2009: +6.2% decade^{-1} in winter +3.6% decade^{-1} in summer	Not wind	1982-2009: small decrease	
Langehaug et al. (2013)			1957-2005: small increase	
Döscher et al. (2014)	Increase	From 1990: ice strength Before 1990: wind	No long-term trend	Decrease
Olason and Notz (2014)	1979-2011: +1.1 km d^{-1} decade^{-1} in summer +0.4 km d^{-1} decade^{-1} in winter	Ice strength		
Krumpen et al. (2016)			1980-2012: significant positive trend	
Smedsrud et al. (2016)	Increase	Wind	1979-2014: +6% decade^{-1}	

Table 2. Mean sea ice thickness h, drift speed D, deformation rates d_r and net ice production p_i temporally averaged over the period 1979-2013 and spatially averaged over the SCICEX box for the five P^* experiments.

P^* (kN m^{-2})	h (m)	D (km d^{-1})	d_r (d^{-1})	p_i (mm d^{-1})
5.5	3.70	7.75	0.0277	1.27
20	2.47	7.96	0.0232	1.38
27.5	2.31	7.73	0.0219	1.41
45	2.16	7.23	0.0205	1.53
100	2.09	6.53	0.0214	0.95